Thermal Analysis of Hot Mix Asphalt Pothole Repair by Finite-Element Method

Juliana Byzyka, Ph.D.[1]; Mujib Rahman, Ph.D.[2]; and Denis Albert Chamberlain, Ph.D.[3]

Abstract: Traditional repair methods tend to suffer from inadequate net interface heating because the combined effect of placing hot fill mix in a cold, old pavement leads to inadequate net temperature levels. The outcome of this is low durability and limited life. In contrast, the outcome of placing hot mix in a controlled, preheated host pavement is substantial increased working life. To understand repair heating, this study ran heat transfer finite-element models for the cases of (1) hot mix asphalt (HMA) placed in an ambient temperature pothole, (2) the heated pothole recess, and (3) HMA placed in the preheated pothole recess. The air–pavement–heater system model comprises a host pavement with two pothole repairs or, in the case of the second thermal model, with one empty pothole excavation, and an infrared heating element plate. For calibration purposes, experimental work of simulated repairs undertaken in previous research was used. The air–pavement–heater system setup followed an optimum pothole preheating method also determined in previous research. Thermal models were validated with previous experimental work. It was concluded that the models generate reasonable transient temperature profiles within the dynamically heated pothole excavation, at the interface of the repairs, and inside the host pavement. **DOI: 10.1061/JPEODX.0000156.**

Introduction

Potholes are one of the most common and severe deteriorations in asphalt pavements and considerably decrease the quality of road conditions. Water and repeated traffic loading are two main factors that accelerate their development. Water permeates through cracks in the asphalt pavement and weakens the cohesive and adhesive bonds of the asphalt matrix under the action of wheel-induced pressure, leading gradually to cracking and raveling and on to the formation of potholes. Furthermore, potholes are considerably increased during the frost and freeze cycles (Lesueur and Youtcheff 2014; Adlinge and Gupta 2013). Cold or hot asphalt mixtures are used to repair potholes (Thom 2008; Advanced Asphalt Technologies, LLC 2011), and common repair methods are pothole filling and patching (Lavin 2003). One of the main failures in patching is interface debonding (Prowell and Franklin 1996), which is caused by uncontrolled pothole repair practices (Byzyka et al. 2017b) that do not respect the thermal characteristics of asphalt.

To increase pothole repair performance and durability, ongoing research suggests preheating the pothole excavation prior to repair using infrared heat. The use and effectiveness of infrared and microwave technology in asphalt repair has been studied by Kandhal and Rao (1994), Clyne et al. (2010), Uzarowski et al. (2011), Williams (2011), Freeman and Epps (2012), Nazzal et al. (2014), and Huang et al. (2016). These studies acknowledge that preheating of the old pavement prior to repair increases the density of the mixture in the repair interface and its adhesion. However, the effect of asphalt's thermophysical properties in repair bonding with the host pavement during static and dynamic repairs has not been reported. Heat flow in asphalt pavement under infrared heat and during repair activity has also not been reported. In this paper, both of these shortcomings are addressed and three repair approaches are investigated using finite-element modeling (FEM).

FEM has been used to simulate temperature distribution in asphalt pavement under a variety of weather conditions, and it has also been used to simulate vehicle load interaction with asphalt pavement (Hadi and Bodhinayake 2003; Hermansson 2004; Akbulut and Aslantas 2005; Minhoto et al. 2005; Yang and Liu 2007; Melaku and Qiu 2015; Li et al. 2018; Han et al. 2018). However, with the exception of Rahman et al. (2013), which presents a preliminary three-dimensional finite-element (FE) repair model, no other studies were found to conduct an FE analysis of pothole repair. Thus, the models reported in this study are necessary because (1) there is currently no such simulation that investigates heat flow in asphalt pothole repair, which could help to overcome the issue of cool repair boundaries; (2) the models could be used in the future to calibrate infrared heaters and to help optimize the use of heaters in asphalt repair under a variety of environmental conditions, repair conditions, repair geometry, and asphalt properties; and (3) the initial development of the static repair model followed by the dynamically heated pothole excavation model helped the authors to build the dynamically heated repair model. The aim is for these simulation models to become part of an integrated repair guideline starting with recognizing the pavement distress on site and progressing to its repair with infrared heat. This is shown in Fig. 1. The objective of this research is to develop a transient thermal parametric hot mix asphalt (HMA) repair model with appropriate parametric options and calibrate the model against an experimental study.

Further, the collection of experimental temperature profiles in static and dynamic repair interfaces and the environmental and other conditions used in this work are described in a previous study (Byzyka et al. 2018a) and were used to validate the respective thermal models and build them accordingly. The thermophysical properties of

[1]Lecturer, School of Science, Engineering and Environment, Univ. of Salford, Manchester M5 4WT, UK (corresponding author). ORCID: https://orcid.org/0000-0002-5570-8909. Email: j.byzyka@salford.ac.uk

[2]Senior Lecturer, Dept. of Civil and Environmental Engineering, Brunel Univ. London, Middlesex UB8 3PH, UK. Email: mujib.rahman@brunel.ac.uk

[3]Professor, Dept. of Civil and Environmental Engineering, Brunel Univ. London, Middlesex UB8 3PH, UK. Email: denis.chamberlain@brune.ac.uk

Note. This manuscript was submitted on November 13, 2018; approved on September 18, 2019; published online on April 23, 2020. Discussion period open until September 23, 2020; separate discussions must be submitted for individual papers. This paper is part of the ***Journal of Transportation Engineering, Part B: Pavements***, ©ASCE, ISSN 2573-5438.

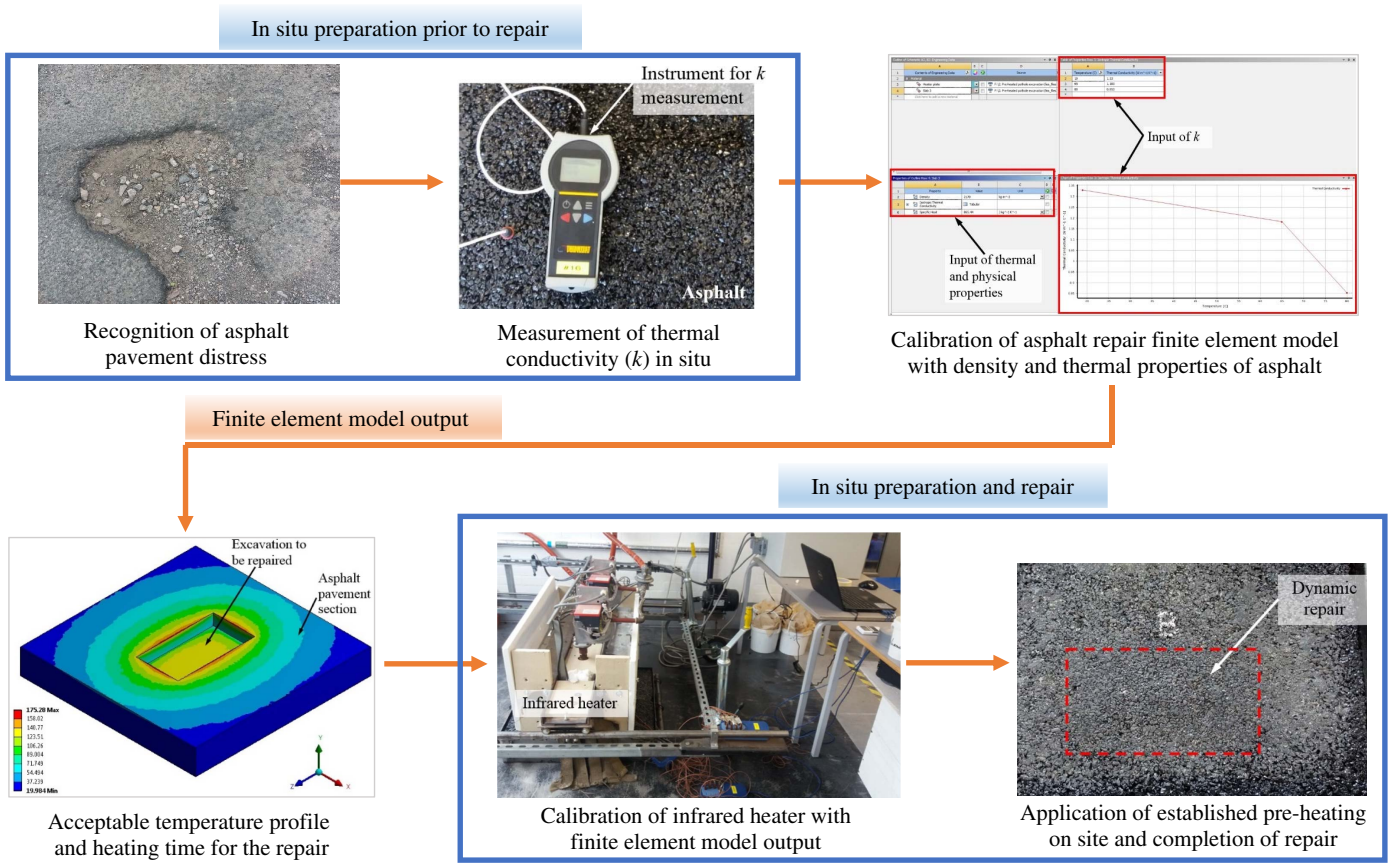

Fig. 1. Integrated asphalt pavement repair.

asphalt mixtures measured from this previous study were input into the models. A similar method from Byzyka et al. (2018b) was followed for the dynamically heated pothole excavation.

Definitions

This paper presents three asphalt thermal models, which are defined as follows:

- Static repair: common practice nonheated repair where heat flows from the new HMA to the cold host pavement;
- Dynamically heated pothole excavation: excavated and clean pothole preheated with infrared heat in heating (heater on)–cooling (heater off) cycles prior to filling with new HMA and compaction; and
- Dynamic repair: preheated repair with dynamic heating prior to filling with new HMA and compaction.

Presented Models

Static and dynamic repair models and a dynamically heated pothole excavation model are presented in this paper. The models simulate temperature distribution in the repair interfaces and on the faces of a pothole excavation under the application of dynamic heating. These simulations were developed using ANSYS software (ANSYS Workbench 2019). A preliminary version of the dynamically heated pothole excavation is published in Byzyka et al. (2017a) but has since undergone significant alterations and improvements. These improvements were applied to all models. Specifically, the thermal and physical properties of the asphalt mixtures were measured in the laboratory and used to calibrate the models. The thermal contact in the repair activities was simulated using thermal contact conductance (TCC). In addition, this paper includes experimental validation of all models, involving a total of 37 temperature point measurements.

Materials and Properties

Three geometries were designed for the simulations: a host asphalt pavement, a pothole fill, and a heating element plate of an experimental infrared heater presented in Byzyka et al. (2017a). The simulated asphalt mixtures were dense graded mixtures with 20-mm maximum aggregate size [commonly known as 20-mm dense bitumen macadam (DBM)] for the host pavement and 6-mm maximum aggregate size [commonly known as asphalt concrete (AC) 6] for the repairs. The investigated density, thermal conductivity, and specific heat capacity of these mixtures were input into the simulations. The thermal conductivity of the mixtures was measured using the transient line method in accordance with Chadbourn et al. (1996) and ASTM (2014) at test temperatures of 19°C, 65°C, and 80°C. Then, specific heat capacity was calculated using Eq. (1) (Hassn et al. 2016). The heater plate properties were taken from the literature (Resistalloy Trading Ltd. 2016). The material properties and parameters for each model are shown in the respective subsequent sections. Eq. (1) is as follows:

$$c_P = \frac{1}{m_{\text{total}}}\left(m_{\text{aggregate}} \cdot c_{\text{aggregate}} + m_{\text{bitumen}} \cdot c_{\text{bitumen}}\right) \quad (1)$$

where c_p = specific heat capacity (J/kg K); m = mass of each material (kg); and c = specific heat capacity of each material (J/kg K).

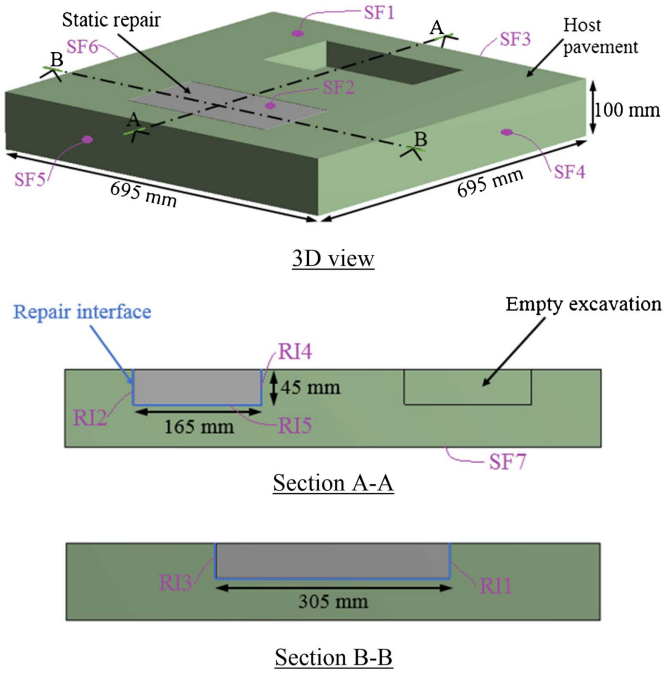

Fig. 2. Static repair three-dimensional geometrical modeling. SF = surface; and RI = repair interface.

Static Repair Model

Model Generation

The model comprises a host pavement 695 × 695 × 100 mm with two pothole excavations 305 × 165 × 45 mm and a pothole fill of similar dimensions to the pothole excavation (Fig. 2). The geometry of the pavement represents the two top layers of a multilayered asphalt pavement designated as surface and binder courses. This two-layered asphalt pavement was idealized in the simulation as homogeneous, continuous, and semi-infinite in the horizontal and vertical directions. The depth of surface and binder courses usually range between 20 and 50 mm and between 50 and 100 mm, respectively (Thom 2008), which justifies the chosen 100-mm depth of the pavement.

Thermal Analysis

Steady-state thermal analysis was used to apply body temperatures and initial air temperature followed by transient thermal analysis to simulate the thermal relationship between the pavement and the pothole repair. Heat energy and radiation exchange between the air and the pavement in the simulation model were defined by applying convection at SF1–SF7 and radiation at SF1 and SF2, respectively (Fig. 2).

Heat conduction at the bonded repair interface was defined by the TCC. TCC is the reciprocal of thermal contact resistance (TCR) and therefore determines the resistance to pavement/repair thermal conduction per unit area at the repair interface (Thompson and Thompson 2007). TCC in the repair activity is influenced by many factors such as contact pressure, interface temperature, heat flow direction, surface oxidation, compaction load cycling, surface cleanliness, surface roughness, surface contact spots, and interstitial zones (Somé et al. 2013; Dou et al. 2016; Frekers et al. 2017). Therefore, TCC plays a significant role in simulating the heat flow and bonding in the repair interfaces.

In this study, the TCC for the vertical repair interfaces was calculated as explained in Straube (2003) for an enclosure assembly. First, the TCC of each asphalt layer of the pavement-repair assembly was calculated using Eq. (2). Then, the TCR of each layer was calculated using Eq. (3). Subsequently, the sum of the individual TCRs was found and used in Eq. (4) to calculate the individual

Table 1. Static repair model parameters

Parameters	Model for prediction of temperatures at the vertical repair interfaces	Model for prediction of temperatures at the bottom repair interface
Air temperature	21.5°C	20.05°C
Pavement temperature prior to repair	25.54°C	20.48°C
Precompaction repair mix temperature	99.73°C	95.70°C
Density of pavement geometry	2,150 kg/m^3	2,150 kg/m^3
Thermal conductivity of pavement geometry	19°C: 1.330 W/m · K 65°C: 1.183 W/m · K 80°C: 0.853 W/m · K	19°C: 1.330 W/m · K 65°C: 1.183 W/m · K 80°C: 0.853 W/m · K
Specific heat capacity of pavement geometry	865.44 J/kg · K	865.44 J/kg · K
Density of repair geometry	2,230 kg/m^3	2,230 kg/m^3
Thermal conductivity of repair geometry	19°C: 1.506 W/m K 65°C: 1.255 W/m K 80°C: 0.937 W/m K	19°C: 1.625 W/m K 65°C: 1.296 W/m K 80°C: 0.963 W/m K
Specific heat capacity of repair geometry	899.46 J/kg · K	899.46 J/kg · K
Convection film coefficient at surfaces SF1–SF7	5 W/m^2	5 W/m^2
Asphalt emissivity (Hermansson 2001)	0.9	0.9
Air–pavement–repair heat flow	Convection applied at SF1–SF7; radiation applied at SF1 and SF2 (Fig. 2).	Convection applied at SF1–SF7; radiation applied at SF1 and SF2 (Fig. 2).
Pavement repair heat flow	Radiation applied at RI1–RI5 (Fig. 2)	Radiation applied at RI1–RI5 (Fig. 2)
TCC	RI1: 2.86 W/m^2 · K; RI2: 5.64 W/m^2 · K; RI3: 2.86 W/m^2 · K; RI4: 4.02 W/m^2 · K; RI5:300 W/m^2 · K	RI1: 2.86 W/m^2 · K; RI2: 5.64 W/m^2 · K; RI3: 2.86 W/m^2 · K; RI4:4.02 W/m^2 · K; RI5: 300 W/m^2 · K
Mesh	Tetrahedrons with midside element nodes	Tetrahedrons with midside element nodes
Total elements	134,487	134,487
Analysis time	480 s	445 s

J. Transp. Eng., Part B: Pavements, 2020, 146(3): 04020029

TCC of the four repair interfaces (R11–R14) of the assembly. The equations are as follows:

$$\text{TCC} = \frac{k}{t} \tag{2}$$

where TCC is expressed in $\text{W/m}^2 \cdot \text{K}$; k = thermal conductivity ($\text{W/m} \cdot \text{K}$); and t = thickness (m), and

$$\text{TCR} = \frac{1}{\text{TCC}} \tag{3}$$

$$\text{TCC} = \frac{1}{\text{TCR}} \tag{4}$$

In addition, the TCC for the bottom repair interface was not calculated but altered until the simulated interlayer temperatures showed no change. This was done because during the compaction of the pothole repair, the contact pressure at the bottom of the repair is expected to be higher than at the sides of the repair. High contact pressure at the interface means high contact conductance but low contact resistance. Table 1 gives the individual TCC of the repair interfaces of the model.

Convergence Study

To ensure a representative model, a mesh convergence test was performed. For the mesh, a finer element size was adopted for the external surfaces of the pothole excavation in the pavement geometry and the repair mixture geometry. The final mesh elements number 134,487. The simulation was run for 480 s of heat transfer, the time taken to place the asphalt mixture in the pothole excavation, evenly spreading and compacting it. Temperatures occurring at the vertical and bottom repair interfaces for the validation of the model were measured for different host pavements and repairs, for different material and air temperatures. Since these parameters were expected to affect the distribution of temperatures in the simulations, two static repair simulation models were similarly developed. The model parameters are presented in Table 1.

Dynamically Heated Pothole Excavation

Model Generation

The model consists of a host pavement 695 × 695 × 100 mm with a pothole excavation 305 × 165 × 45 mm and a heating element plate 455 × 165 × 10 mm (Fig. 3). According to the optimum pre-heating method based on previous work (Byzyka et al. 2018b) and mentioned in the "Introduction," the heater is stationary above the pothole excavation and offset at 230 mm, heat is applied in heating–cooling cycles, and the heater operates with 6.6-kW heating power for the heating part of the cycles. This dynamic heating is applied for 615 s and is described in the subsequent sections.

To simulate the operation of the heater, the heating element plate geometry was designed with 12 bonded three-dimensional sections (S1–S12) (Fig. 3). Temperatures from each section were measured in the laboratory and input at the bottom surface of the simulation geometries S1–S12. The heating element plate of the actual heater is a continuous plate. However, its division in the simulation model helped to better correlate the temperature nonlinearity and unevenness between S1 and S12 when operating at 6.6-kW heat power. To simulate the application of infrared heat from the heater to the pothole excavation, radiation was applied at the faces of the excavation, at the pavement top surface, and on the bottom faces of the heating element plate.

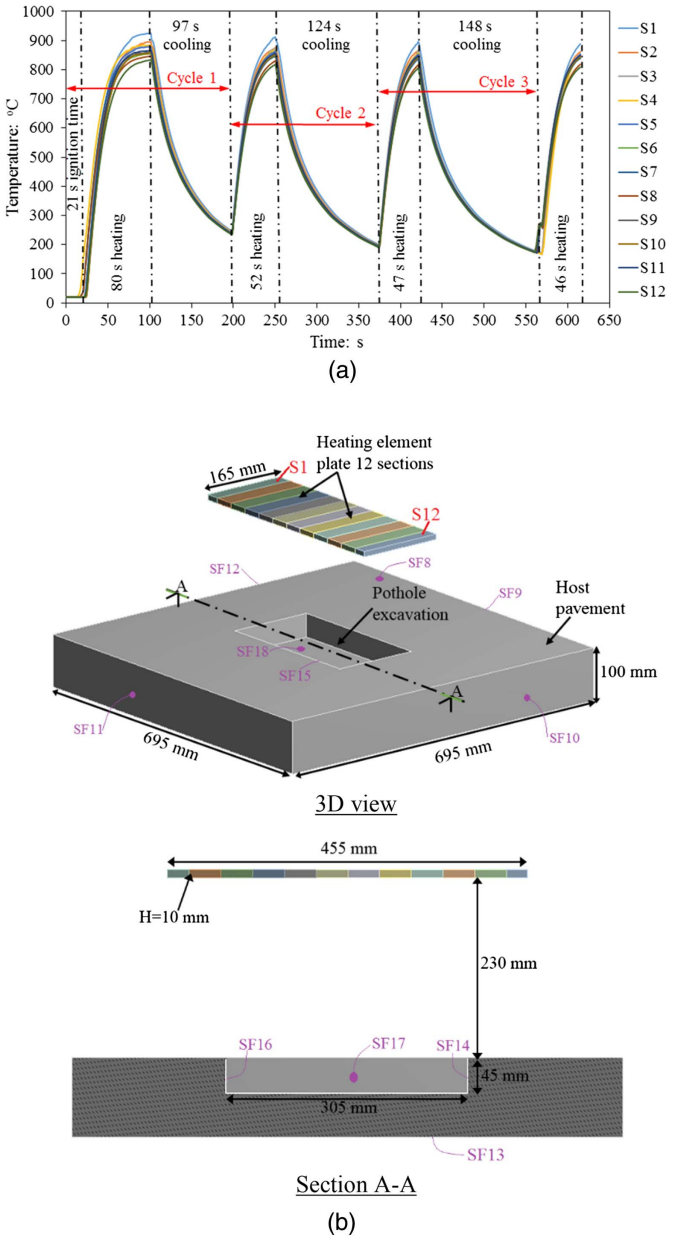

Fig. 3. Dynamically heated pothole excavation model: (a) temperature distribution on heating element plate for Sections S1–S12; and (b) three-dimensional geometrical modeling. SF = surface; and RI = repair interface.

Thermal Analysis

Steady-state and transient analysis were used to build this model, with a convected air temperature of 22.3°C applied at surfaces SF8–SF13. Convection at air temperatures of 120°C, 160°C, and 180°C were applied at the bottom of the pothole excavation (SF18) and at faces SF15–SF17 and SF14–SF16, respectively [Fig. 3(b)]. This was done to provide close correlation between simulated and measured temperatures under infrared heat. The main issue is that the vertical faces of the excavation are not as exposed to the heater plate as the bottom face. This means that the temperatures of the vertical faces as calculated by the simulation could possibly be lower than temperatures measured in the repairs performed in the laboratory. This may happen because the surface-to-surface radiation algorithm used by ANSYS software incorporates view factor

calculations, which take into account how much radiative heat can be transmitted to the surfaces defined within an enclosure. Further, in practice, due to the presence of convection, it is likely that the vertical surfaces of the pothole will be heated due to their proximity to the base of the excavation and the heat being convected from that surface.

Convergence Study

A mesh convergence test was also performed. For the mesh, a finer element size was adopted for the faces of the pothole excavation in the pavement geometry and on the bottom faces of the heating element plate. The final mesh elements number 52,967. The simulation was run for 615 s according to the optimum laboratory heating method previously described. The model parameters are given in Table 2.

Experimental Procedure for Measuring Temperatures on a Heating Element Plate

Temperatures were measured at 36 temperature sampling points on the heating element plate using a 1.5-m long insulated thermocouple probe connected to a data logger. The probe is capable of measuring temperatures up to 1,335°C (accuracy ±1.1°C or 0.4%, whichever is greater). Temperatures were measured for a duration of 615 s of dynamic heating with the heater set at 6.6-kW heat power. The ambient temperature ranged between 18°C and 22°C. A preliminary version of this experimental method was published in Byzyka et al. (2017a) but has since undergone refinements to capture the precise distribution of plate temperatures. These alterations are the number of temperature sampling points, the temperature probe used for the measurements, and the time duration of the measurements. The plate temperatures measured in the laboratory experiment [Fig. 3(a)] were input into the dynamically heated pothole excavation and dynamic repair models.

Table 2. Model parameters for dynamically heated pothole excavation

Parameters	Values
Air temperature	22.3°C
Pavement temperature prior to heating	19.86°C
Heating element plate temperature prior to heater operation	18.89°C
Density of pavement geometry	2,150 kg/m^3
Thermal conductivity of pavement geometry	19°C: 1.330 W/m · K 65°C: 1.183 W/m · K 80°C: 0.853 W/m · K
Specific heat capacity of pavement geometry	865.44 J/kg · K
Density of heating element plate (Resistalloy Trading Ltd. 2016)	7,220 kg/m^3
Thermal conductivity of heating element plate (Resistalloy Trading Ltd. 2016)	20°C: 16
Specific heat capacity of heating element plate (Resistalloy Trading Ltd. 2016)	460 J/kg · K
Convection film coefficient at SF8–SF18	5 W/m^2
Asphalt emissivity (Hermansson 2001)	0.9
Heating element plate emissivity	0.9
Air–pavement–heater heat flow	Convection at 22.3°C applied at SF8–SF13 Radiation applied at SF8
Pothole excavation heat flow	Convection at 120°C applied at SF18 Convection at 160°C applied at SF15 and SF17 Convection at 180°C applied at SF14 and SF16 Radiation applied at SF14–SF18
Mesh	Tetrahedrons with midside element nodes
Total elements	52,967
Analysis time	615 s

Dynamic Repair Model

This model was built combining the static repair and the dynamically heated pothole excavation models (Fig. 4). Therefore, the design of the geometries, the position of the heater above the pavement, the material properties, and the simulation model parameters are identical. The difference is in the repair mixture temperature and simulation time. The simulation built to validate temperatures at the vertical repair interfaces was run for 1,095 s in total (615 s preheating of pothole excavation +480 s dynamic repair simulation time). The simulation built to validate temperatures at the bottom repair interface was run for 1,054 s (615 s preheating of pothole excavation +439 s dynamic repair simulation time).

In the simulations, the elements of the dynamic pothole repair geometry were set to an extremely soft stiffness for 615 s to allow excavation preheating to take place without any interaction with the repair geometry. The stiffness was then restored at the end of the preheating period for 480 or 439 s, depending on the simulation run at the time. The initial temperatures of the repair mixtures for these simulations were set at 107°C and 98.3°C, respectively. The final mesh elements number 432,382.

Results

Static Repair Model

Fig. 5 shows the temperature profile over time at 11 sampling points at the interfaces of a 45-mm deep static repair. Simulated temperatures are compared against temperatures measured in laboratory experiments. Thermocouples T1–T6 show temperatures in the vertical sides middepth of the repair for a simulated and experimental repair time of 480 s. Thermocouples T7–T11 show temperatures at the corners and bottom of the repair for a simulated and experimental repair time of 445 s. The exact positions of the thermocouples are determined by previous work (Byzyka et al. 2018a), as stated in the "Introduction." The data used to validate the static

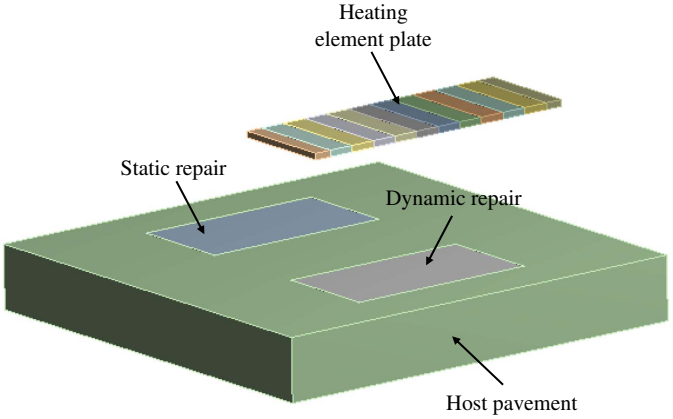

Fig. 4. Dynamic repair three-dimensional geometrical modeling.

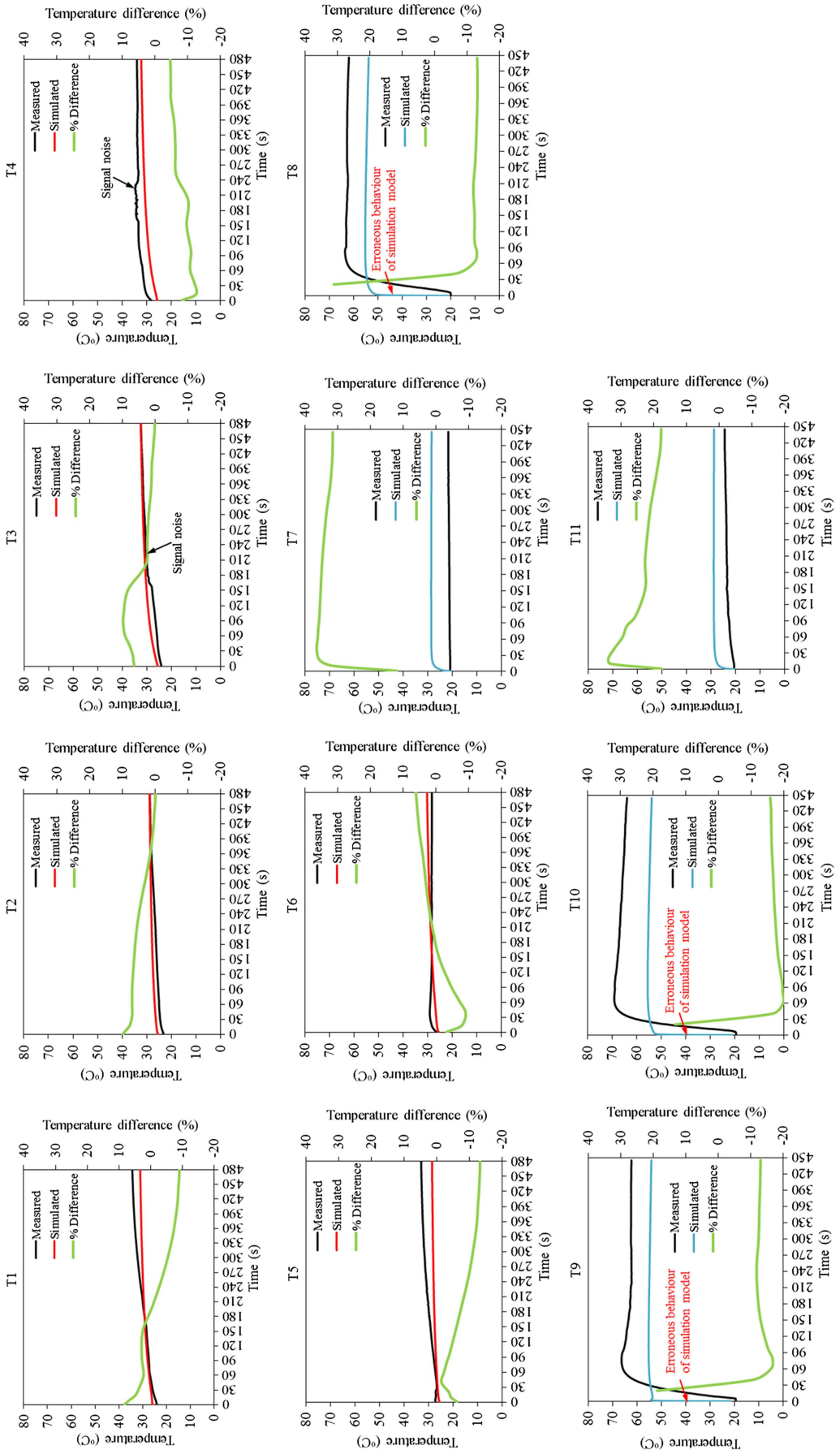

Fig. 5. Comparison of simulated and measured temperatures at the interfaces of static repair.

J. Transp. Eng., Part B: Pavements, 2020, 146(3): 04020029

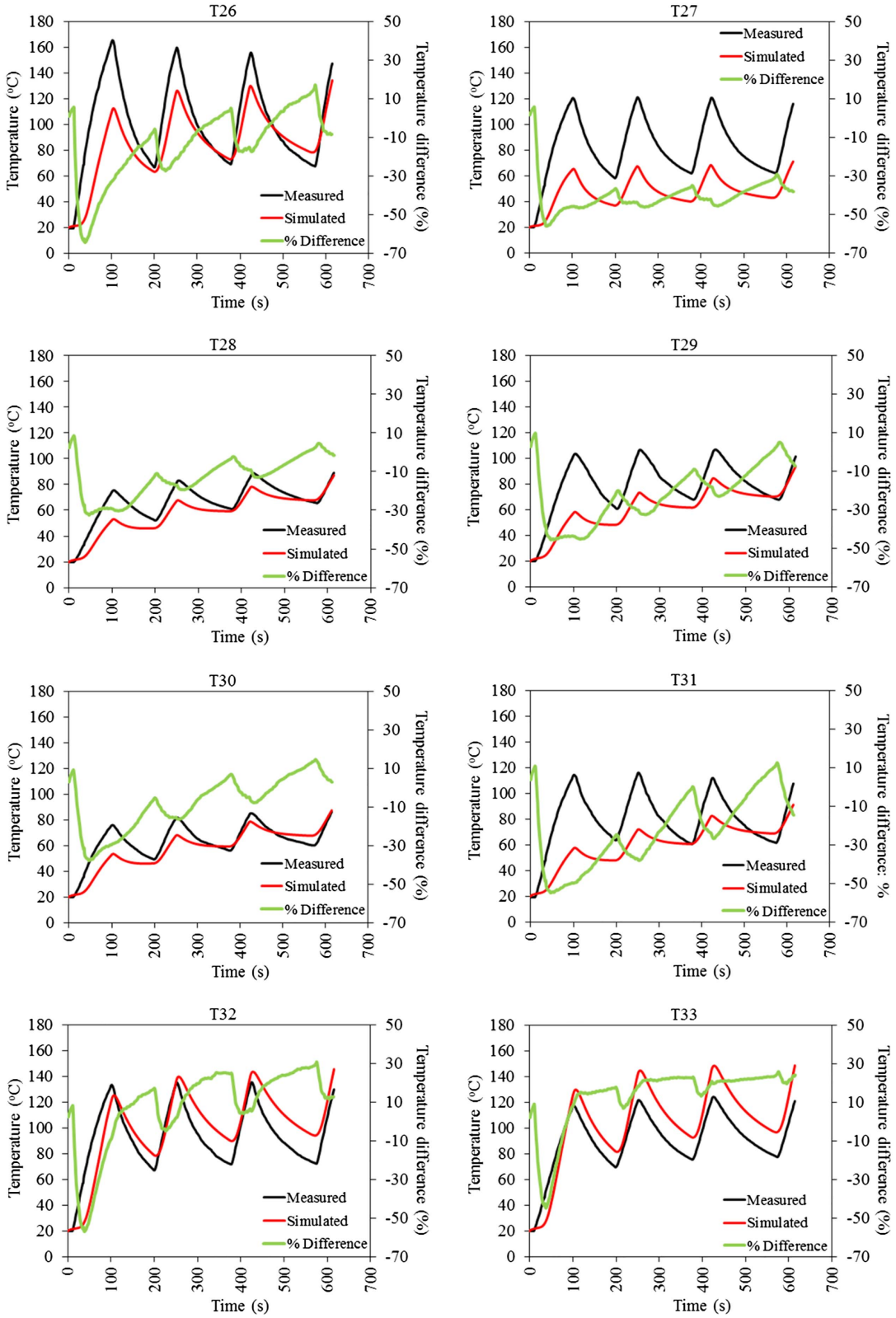

Fig. 6. Comparison of simulated and measured temperatures at the faces of dynamically heated pothole excavation.

repair model were taken from one laboratory repair procedure for each thermocouple group, although six repetitions were performed in the laboratory for each temperature sampling point. However, this was done because the experimental study concluded that temperatures were similarly increased for repairs conducted when air and host pavement temperatures ranged from 17°C to 22°C and from 17°C to 26°C, respectively. The same air and pavement temperatures were used in the simulation.

The results showed that at T1–T6 there was on average 94.53%, 95.52%, 95.62%, 91.83%, 95.52%, and 95.07% correlation,

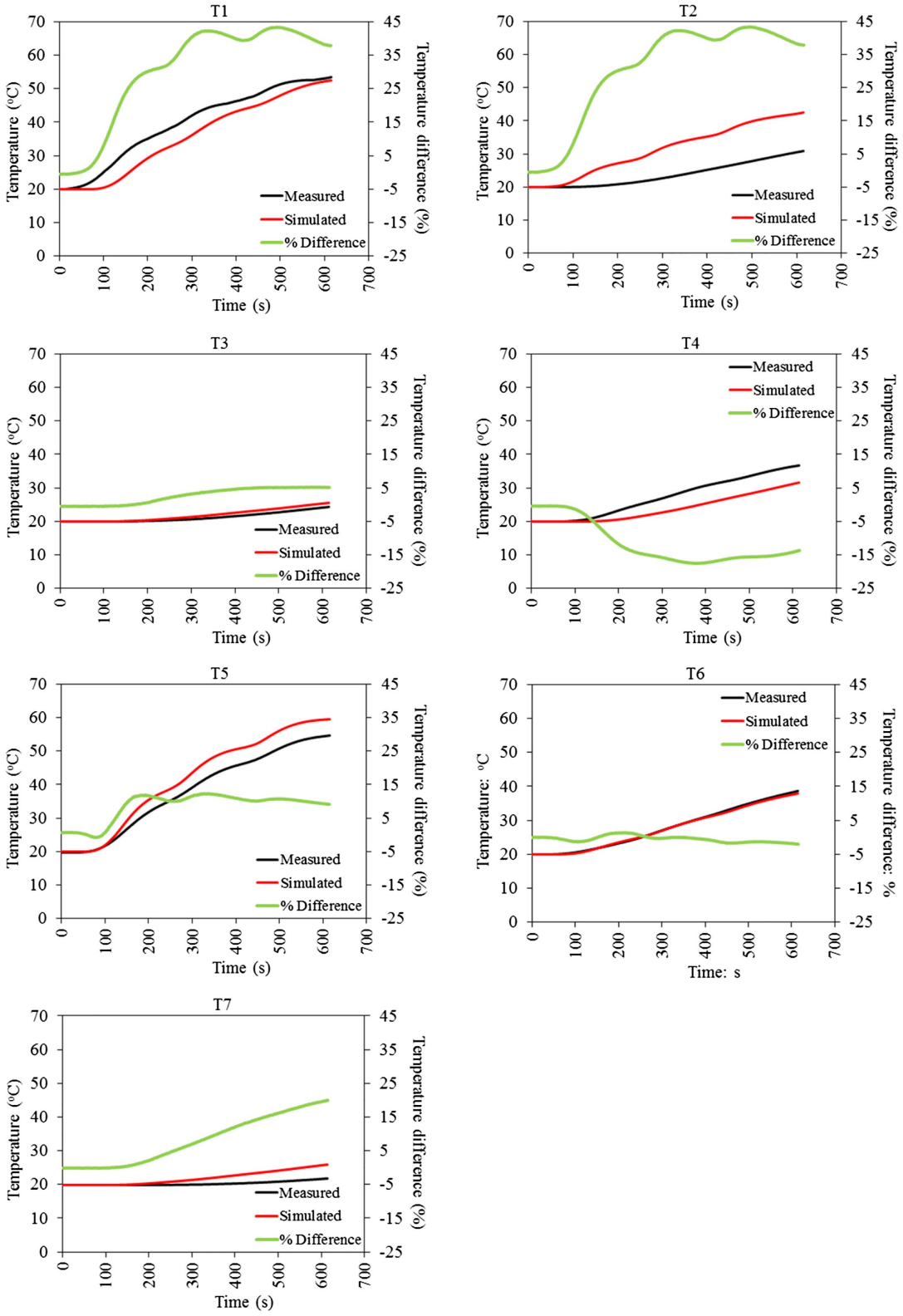

Fig. 7. Comparison of simulated and measured temperatures inside the host pavement of dynamically heated pothole excavation.

respectively, between measured and simulated temperatures. The highest temperature differences were observed at T7 and T11, which were located at two corners at the bottom of the repair. In these locations, correlations of 67.50% and 75.97% between simulated and test data were observed. Temperature prediction improved for T8–T10, located at midbottom areas of the repair interface, where simulated temperatures agreed, on average, with the test temperatures by 86.51%, 86.23%, and 83.00%, respectively. Also at these locations (T8–T10), an error was observed for the first 10 s of the simulation. Specifically, recorded temperatures increased rapidly from approximately 21°C to 55°C, whereas laboratory temperatures measured at the same locations increased from

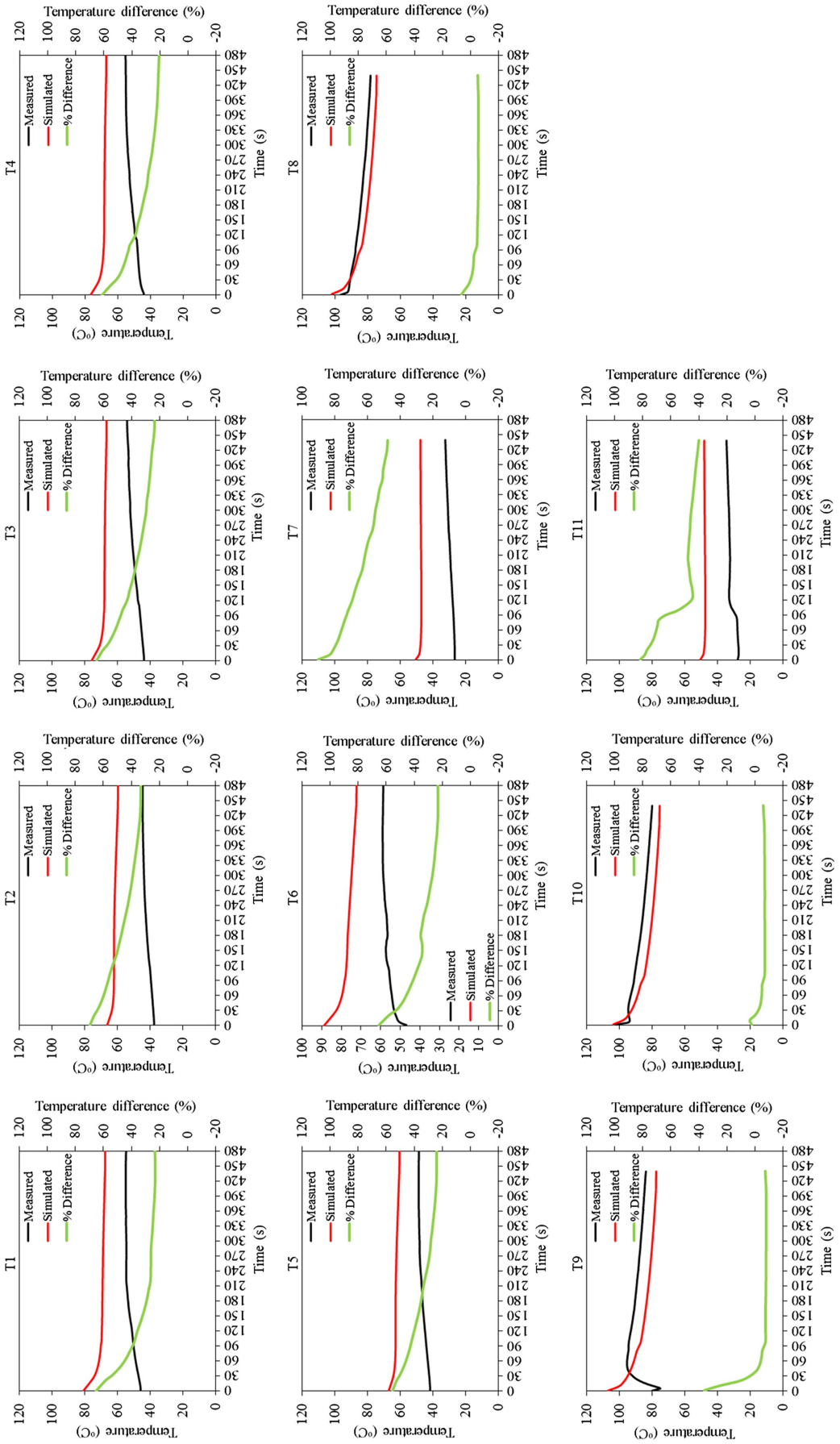

Fig. 8. Comparison of simulated and measured temperatures at the interfaces of dynamic repair.

approximately 20°C to 27°C. For this reason, no correlation of data is included in Fig. 5 for T8–T10 for the first 10 s of simulation time.

Dynamically Heated Pothole Excavation Model

The results and validation of this model are presented in Figs. 6 and 7. In these figures, the characterization and locations of the thermocouples follow that of the experimental work. In Fig. 6, estimated temperatures at eight locations in the pothole excavation are compared against laboratory measurements. Considering the three-dimensional view of the model in Fig. 3, T26 and T27 are located at the midbottom and the bottom corner of the cavity, respectively. Thermocouples T28–T31 are located at the middle of each vertical excavation face, and T32 and T33 are located at mid-top points of the cavity. In Fig. 7, seven more sampling points are presented. They were used to validate simulated temperatures at points located inside and across the depth of the host pavement at a distance from the excavation's long and short faces of 20 ± 5 mm and 30 ± 13 mm, respectively.

Simulated temperatures at T26 and T28–T33 reached an average agreement of 83.29%, 86.51%, 77.53%, 87.71%, 75.85%, 81.93%, and 80.52%, respectively, with the measured temperatures. A lower correlation was observed for T27, with simulated temperatures matching test data by only 59.63% on average. The figure improves for temperatures predicted at locations inside the host pavement during the dynamic heating of the pothole excavation. Specifically, on average, at T1 and T3–T7 correlations of 89.59%, 97.15%, 88.40%, 91.45%, 99.15%, and 91.88%, respectively, were observed. The lowest agreement (69.60%) between simulation and experimental work was seen at T2.

Dynamic Repair Model

This model simulates temperatures over time at the interfaces of a 45-mm deep repair that was dynamically heated prior to fill and compaction. The results are shown in Fig. 8. Thermocouples T1–T6 show temperatures at the vertical sides mid-depth of the repair for a simulated and experimental repair time of 1,095 s. Thermocouples T7–T11 show temperatures at the corners and bottom of the repair for a simulated and experimental repair time of 1,054 s. In comparison to the static repair model, this model has a low correlation between simulated and measured temperatures because the simulated temperatures at the repair interfaces are to some degree affected by the temperatures achieved during the preheating of the excavation. Therefore, for T1–T6 for the first 30 s of repair time, there was an overall average agreement of 40.77%. This figure almost doubled for the repair time between 40 and 480 s and was equal to 64.92%. However, the bottom temperatures measured at Thermocouples T8–T10 had correlations of 95.70%, 91.36%, and 94.34%. The model fails to accurately simulate bottom corner temperatures where, for T7 and T11, agreements of 34.65% and 44.96%, respectively, were seen.

Conclusions

Three simulation models were presented in this study. The pothole repair models and the heated excavation model were a representation of experimental work conducted by the authors. All models were validated and calibrated by the authors' experimental work (Byzyka et al. 2017a, 2018a, b) and form a platform for the future development of an integrated repair guideline beginning with the excavation of pavement distress and culminating in its repair with infrared heat (Fig. 1). This study produced the following conclusions:

- The results of the model validation are promising, and good correlation was found for most investigated temperature sampling points located at the repair interfaces, at the faces of the empty pothole excavations, and inside the host pavement.
- The lowest agreement between measured and simulated temperatures was seen in the dynamic repair model, mainly at the vertical faces of the repair. This is because the simulated temperatures were affected by the dynamically heated pothole excavation, where the lowest agreement between measured and simulated temperatures was also seen at the vertical faces of the excavation.
- TCC plays an important role in simulating heat flow at the repair interface, and view factor significantly affects simulation of temperatures at faces subjected to radiation. TCC is the reciprocal of thermal contact resistance, and its effect on the repair interface temperatures was also underlined in this paper.

Data Availability Statement

Some or all data, models, or code generated or used during the study are available in a repository or online in accordance with funder data retention policies:

Byzyka, J. 2020. "Laboratory and simulation results of static and dynamic pothole repairs." University of Salford Manchester. https://doi.org/10.17866/rd.salford.10289339.v1.

Acknowledgments

This work was supported by International Chem-Crete Corporation, Texas; the Engineering and Physical Sciences Research Council (EPSRC); Brunel University; Epicuro Ltd.; and DAC Consulting (UK) Ltd.

References

Adlinge, S. S., and A. Gupta. 2013. "Pavement deterioration and its causes." *Int. J. Innovative Res. Dev.* 2 (4): 437–450.

Advanced Asphalt Technologies, LLC. 2011. *A manual for design of hot mix asphalt with commentary.* NCHRP Rep. 673. Washington, DC: Transportation Research Board.

Akbulut, H., and K. Aslantas. 2005. "Finite element analysis of stress distribution on bituminous pavement and failure mechanism." *Mater. Des.* 26 (4): 383–387. https://doi.org/10.1016/j.matdes.2004.05.017.

ASTM. 2014. *Standard test method for determination of thermal conductivity of soil and soft rock by thermal needle probe procedure*. ASTM D5334. Washington, DC: ASTM.

Byzyka, J., D. A. Chamberlain, and M. Rahman. 2017a. "Development of advanced temperature distribution model in hot-mix asphalt patch repair." *Proc. Inst. Civ. Eng. Transp.* 172 (4): 199–209. https://doi.org/10.1680/jtran.17.00022.

Byzyka, J., M. Rahman, and D. A. Chamberlain. 2017b. "Thermal segregation of asphalt material in road repair." *J. Traffic Transp. Eng. (English Edition)* 4 (4): 360–371. https://doi.org/10.1016/j.jtte.2017.05.008.

Byzyka, J., M. Rahman, and D. A. Chamberlain. 2018a. "An improved interface temperature distribution in shallow hot mix asphalt patch repair using dynamic heating." *Int. J. Pavement Eng.* https://doi.org/10.1080/10298436.2018.1559315.

Byzyka, J., M. Rahman, and D. A. Chamberlain. 2018b. "An innovative asphalt patch repair pre-heating method using dynamic heating." *Constr. Build. Mater.* 188 (Nov): 178–197. https://doi.org/10.1016/j.conbuildmat.2018.08.086.

Chadbourn, B. A., J. A. Luoma, D. E. Newcomb, and V. R. Voller. 1996. "Consideration of hot mix asphalt thermal properties during

compaction." In *Quality management of hot mix asphalt*, edited by Dale S. Decker, 127–141. West Conshohocken, PA: ASTM. https://doi.org/10.1520/STP16312S.

Clyne, T. R., E. N. Johnson, and B. J. Worel. 2010. *Use of taconite aggregates in pavement applications*. Rep. No. MN/RC-2010-24. St. Paul, MN: Minnesota DOT.

Dou, R., T. Ge, X. Liu, and Z. Wen. 2016. "Effects of contact pressure, interface temperature, and surface roughness on thermal contact conductance between stainless steel surfaces under atmosphere condition." *Int. J. Heat Mass Transfer* 94 (Mar): 156–163. https://doi.org/10.1016/j.ijheatmasstransfer.2015.11.069.

Freeman, T. J., and J. A. Epps. 2012. *HeatWurx patching at two locations in San Antonio*. Rep. No. FHWA/TX-12/5-9043-01-1. College Station, TX: Texas Transportation Institute.

Frekers, Y., T. Helmig, E. M. Burghold, and R. Kneer. 2017. "A numerical approach for investigating thermal contact conductance." *Int. J. Therm. Sci.* 121 (Nov): 45–54. https://doi.org/10.1016/j.ijthermalsci.2017.06.026.

Hadi, M. N. S., and B. C. Bodhinayake. 2003. "Non-linear finite element analysis of flexible pavements." *Adv. Eng. Software* 34 (11–12): 657–662. https://doi.org/10.1016/S0965-9978(03)00109-1.

Han, D., G. Zhu, H. Hu, and L. Li. 2018. "Dynamic simulation analysis of the tire-pavement system considering temperature fields." *Constr. Build. Mater.* 171 (May): 261–272. https://doi.org/10.1016/j.conbuildmat.2018.03.071.

Hassn, A., M. Aboufoul, Y. Wu, A. Dawson, and A. Garcia. 2016. "Effect of air voids content on thermal properties of asphalt mixtures." *Constr. Build. Mater.* 115 (Jul): 327–335. https://doi.org/10.1016/j.conbuildmat.2016.03.106.

Hermansson, Å. 2001. "Mathematical model for calculation of pavement temperatures: Comparison of calculated and measured temperatures." *Transp. Res. Rec.* 1764 (1): 180–188. https://doi.org/10.3141/1764-19.

Hermansson, Å. 2004. "Mathematical model for paved surface summer and winter temperature: Comparison of calculated and measured temperatures." *Cold Reg. Sci. Technol.* 40 (1–2): 1–17. https://doi.org/10.1016/j.coldregions.2004.03.001.

Huang, K., T. Xu, G. Li, and R. Jiang. 2016. "Heating effects of asphalt pavement during hot in-place recycling using DEM." *Constr. Build. Mater.* 115: 62–69. https://doi.org/10.1016/j.conbuildmat.2016.04.033.

Kandhal, P. S., and S. S. Rao. 1994. *Evaluation of longitudinal joint construction techniques for asphalt pavements (Michigan and Wisconsin projects-interim report)*. NCAT Rep. No. 94-01. Auburn, AL: National Center for Asphalt Technology, Auburn Univ.

Lavin, P. 2003. *Asphalt pavements: A practical guide to design, production and maintenance for engineers and architects*. London: Spon Press.

Lesueur, D., and J. Youtcheff. 2014. "Asphalt pavement durability." In *Environmental degradation of advanced and traditional engineering materials*, edited by Lloyd H. Hihara, Ralph P. I. Adler, and Ronald M. Latanision. Boca Raton, FL: CRC Press.

Li, Y., L. Liu, and L. Sun. 2018. "Temperature predictions for asphalt pavement with thick asphalt layer." *Constr. Build. Mater.* 160 (Jan): 802–809. https://doi.org/10.1016/j.conbuildmat.2017.12.145.

Melaku, S., and H. Qiu. 2015. "Finite element analysis of pavement design using ANSYS finite element code." In *Proc., 2nd Int. Conf. on Civil Engineering, Energy and Environment*, 64–69. Hubei, China: Wuhan Univ. of Technology.

Minhoto, M. J. C., J. C. Pais, P. A. A. Pereira, and L. G. Picado-Santos. 2005. "Predicting asphalt pavement temperature with a three-dimensional finite element method." *Transp. Res. Rec.* 1919 (1): 96–110. https://doi.org/10.1177/0361198105191900111.

Nazzal, M. D., S. Kim, and A. R. Abbas. 2014. *Evaluation of winter pothole patching methods*. Rep. No. FHWA/OH-2014/2. Columbus, OH: Ohio DOT, Office of Statewide Planning and Research.

Prowell, B., and A. Franklin. 1996. "Evaluation of cold mixes for winter pothole repair." *Transp. Res. Rec.* 1529 (1): 76–85. https://doi.org/10.1177/0361198196152900110.

Rahman, M. M., J. R. A. Grenfell, S. J. Arulanandam, and A. Ianakiev. 2013. "Influence of thermal segregation on asphalt pavement compaction." *Transp. Res. Rec.* 2347 (1): 71–78. https://doi.org/10.3141/2347-08.

Resistalloy Trading Ltd. 2016. "Fecralloy properties: Physical and mechanical properties." Accessed June 14, 2016. http://www.resistalloytrading.co.uk/pages/fecralloyproperties.

Somé, S. C., D. Delaunay, and V. Gaudefroy. 2013. "Comparison and validation of thermal contact resistance models at solid–liquid interface taking into account the wettability parameters." *Appl. Therm. Eng.* 61 (2): 531–540. https://doi.org/10.1016/j.applthermaleng.2013.08.032.

Straube, J. F. 2003. "Heat flow basics, 2000–2003." Accessed January 14, 2020. http://www.civil.uwaterloo.ca/beg/arch264/arch264%20heat%20flow%20basics.pdf.

Thom, N. 2008. *Principles of pavement engineering*. London: ICE Publishing.

Thompson, M. K., and J. M. Thompson. 2007. "Considerations for predicting thermal contact resistance in ANSYS." In *Proc., 17th KOREA ANSYS User's Conf.* Cheongju, Korea.

Uzarowski, L., V. Henderson, M. Henderson, and B. Kiesswetter. 2011. "Innovative infrared crack repair method." In *Proc., 2011 Annual Conf. and Exhibition of the Transportation Association of Canada. Transportation successes: Let's Build on Them. 2011 Congress Et Exhibition De l'Association Des Transports Du Canada. Les Succes En Transports: Une Tremplin Versl'Avenir.* Edmonton, AB: Transportation Association of Canada.

Williams, S. G. 2011. *HMA longitudinal joint evaluation and construction*. Rep. No. TRC-0801. Little Rock, AR: Univ. of Arkansas.

Yang, X., and B. Liu. 2007. "Coupled-field finite element analysis of thermal stress in asphalt pavement." *J. Highway Transp. Res. Dev. (English Edition)* 2 (1): 1–6. https://doi.org/10.1061/JHTRCQ.0000158.